ELSEVIER

Journal of Nuclear Materials 299 (2001) 9–19

journal of nuclear materials

www.elsevier.com/locate/jnucmat

Analytical method for thermal stress analysis of plasma facing materials

J.H. You *, H. Bolt

Max-Planck-Institut für Plasmaphysik, EURATOM Association, Boltzmannstr. 2, D-85748 Garching, Germany

Received 10 May 2001; accepted 1 August 2001

Abstract

The thermo-mechanical response of plasma facing materials (PFMs) to heat loads from the fusion plasma is one of the crucial issues in fusion technology. In this work, a fully analytical description of the thermal stress distribution in armour tiles of plasma facing components is presented which is expected to occur under typical high heat flux (HHF) loads. The method of stress superposition is applied considering the temperature gradient and thermal expansion mismatch. Several combinations of PFMs and heat sink metals are analysed and compared. In the framework of the present theoretical model, plastic flow and the effect of residual stress can be quantitatively assessed. Possible failure features are discussed.

1. Introduction

1.1. Thermal stresses in plasma facing components

The quasi-stationary surface high heat flux (HHF) from the fusion plasma to in-vessel components such as first wall or divertors is a basic loading mode on plasma facing materials (PFMs) during the normal operation of thermonuclear reactors [1]. Typically, in fusion devices with long plasma discharges the PFMs will be bonded to a metallic heat sink. This heat sink is furnished with coolant channels for the heat removal. Thus the incident heat flux will be conducted through the thickness of the PFM and through the interface into the heat sink structure.

This thermal load generates secondary stresses in the plasma facing components. Firstly, the difference in the coefficient of thermal expansion (CTE) of the constituting materials causes a significant misfit stress especially in the region near bond interfaces between PFM and heat sink material [1,2]. The thermal stress induced from the mismatch of the CTEs is controlled by the change of temperature at the bond interface from the stress free state [3]. Such a mismatch stress can be generated even during the manufacturing process of joints resulting in residual stress within the joint [4]. The subsequent stress from the thermal loading during operation will be superposed on this residual stress field. In the presence of the residual stress, heating of the joint will lead to a reduction of the misfit stress, if the plastic flow is not dominant [5].

Secondly, the temperature gradient developing in the PFM produces an additional thermal stress [6]. During the start-up phase, the initial temperature evolution will be transient and the temperature distribution will show a steep curvilinear profile. After reaching the steady state, the temperature profile turns into a slope which deviates from a linear profile only depending on the temperature dependence of thermal conductivity. The corresponding thermal stress in the PFM increases gradually having a similar profile as that of the temperature, if yielding has not occurred yet. For materials having a high elastic modulus or high CTE, this contribution can be comparable to those from the misfit of the thermal expansion.

1.2. Motivation

To obtain the reliable structural integrity, the selection of the proper material combinations, an optimised

* Corresponding author. Tel.: +49-89 3299 1373; fax: +49-89 3299 1212.

E-mail address: jeong-ha.you@ipp.mpg.de (J.H. You).

0022-3115/01/$ - see front matter
PII: S0022-3115(01)00674-2

component design and the estimation of the load limit are required. From the mechanical point of view, the interplay of the thermal stress of PFMs and their inherent resistance to mechanical failure is an essential concern to assess the performance of the candidate materials. To this end, a comparative analysis of the stress state of PFCs for various relevant material combinations is required.

The exact computation of stress fields needs, of course, consideration of the detailed component geometry and realistic loading history. In addition, the temperature dependence of material properties should not be neglected. To meet these requirements, numerical methods such as the finite element analysis is commonly used, since the complicated boundary conditions and the temperature dependent properties can hardly be handled in a fully analytical framework.

However, a simplified analytical estimation can provide us with a comprehensive insight into the thermomechanical behaviour of plasma facing materials and components. Due to required simplification and generalisation, it will be essentially semi-quantitative. In any case, such an analytical approach could be effectively applied to the materials screening procedure prior to a detailed structural design which may require an extensive computational effort. Such analytical solutions will show the clear correlation between the involved parameters. The purpose of this work is to provide comprehensive analytical tools to estimate the thermal stress of actively cooled PFMs under fusion relevant loading conditions.

In what follows, analytical modelling for the thermal stress of actively cooled plasma facing components is presented. The stress analysis is performed only for the plasma facing armour tiles. The stress state within the metallic heat sink will not be given here, since it depends more strongly on a specific design configuration.

Finally, test results for several important material combinations are presented. A possible failure mechanism is discussed.

2. Some remarks on the analysis

2.1. Assumptions

In this article, the stress analysis is restricted only to the plasma facing armour tiles, though the reaction force of the substrate is, of course, included in the analysis.

The PFMs for the armour tile are assumed to be linear-elastic whereas the metals for the heat sink substrate be elastic and perfect-plastic.

The instantaneous thermal stress of PFMs will be significantly influenced by the local plastic flow of the metallic substrate beneath the bond interface, if it occurs. The extent of the influence of this stress relaxation on the misfit stress in the armour tile will surely be dominated by the flow stress of the substrate. The plastic yielding of the metallic substrate is taken into account for the analysis. In Section 7, results of the elasto-plastic analysis are compared with those of a linear-elastic one. Such systems can directly be applied to joint components consisting of brittle armour tiles and metallic heat sink substrates.

Since the purpose of this article is not to predict exact temperature or stress values but to present an analytical scheme for a reasonable estimation of thermal stresses of PFMs, the simplification of boundary condition and load case is made without losing the essential feature of loading characteristics of surface-heat-flux loaded PFCs of fusion reactors. In the same sense, the temperature dependence of the material properties (both thermal and mechanical) is neglected for the sake of brevity. All results presented in this work are obtained for the steady state. Furthermore, the temperature field in the heat sink substrate is assumed to be uniform, which would be a rough approximation for materials having a relatively small heat conductivity.

2.2. The method of stress superposition

As stated in the introduction already, there are two sources of thermal stress, which are expected to be generated in the actively cooled armour tiles under HHF loading. If each case can be treated as a separate problem with proper boundary condition, the stress analysis will be more concise and clear. According to the principle of stress superposition, these thermal stress contributions can be linearly superposed to give the resultant total stress σ_1^{total}, provided the armour tile materials remain in the elastic regime [6].

The concept of the stress superposition method is shown in Fig. 1. The model structures stand for the symmetric half of a PFC joint. It is shown that a PFM armour tile is bonded to the heat sink substrate which contains a coolant channel.

A typical temperature profile in this representative PFC geometry is plotted in the figure. Following the aforementioned assumption that the temperature in the heat sink is uniform being equal to T_0, the substrate will impose two kinds of mechanical constraints, that is, against in-plane thermal expansion and bending.

Figs. 1(b) and (c) on the right-hand side show two imaginary constituent boundary conditions which represent two possible stress sources, respectively. Fig. 1(b) indicates the boundary condition for the stress term σ_1^{HHF} being induced by the temperature profile building in the armour tile under bonding constraint by the substrate. It should be noted that the lowest temperature starts from 0 °C instead of T_0. This is due to the fact that it is just the relative temperature difference along the armour tile thickness that determines the thermal stress

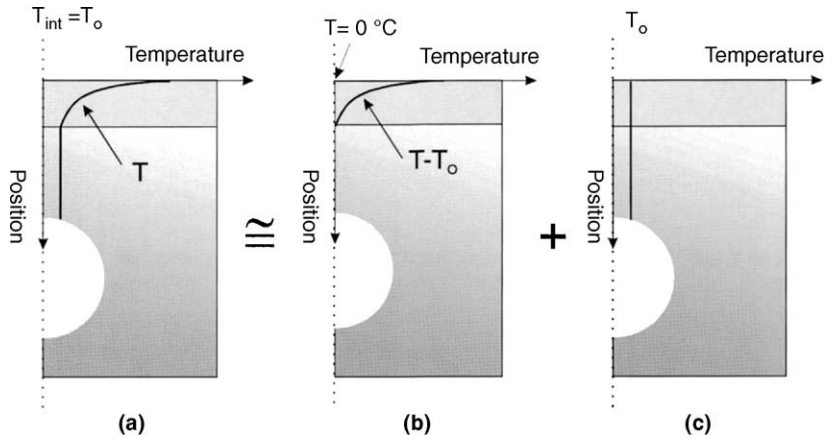

Fig. 1. Schematic of the stress superposition method used for the analysis. Each illustration represents the mechanical boundary conditions with the corresponding imaginary temperature profiles. Only the symmetric half of a component cross-section is shown.

generated by the temperature gradient as long as the substrate temperature is uniform.

Fig. 1(c) stands for the boundary condition which is responsible for the generation of the mismatch stress $\sigma_1^{\text{mismatch}}$ for the interface temperature T_0. Here, a uniform temperature field is assumed.

In short, the superposition method is summarised as

$$\sigma_1^{\text{total}} = \sigma_1^{\text{HHF}} + \sigma_1^{\text{mismatch}}. \quad (1)$$

At first, the thermal stress portion σ_1^{HHF} is considered in Section 4. The thermal stress portion $\sigma_1^{\text{mismatch}}$ is discussed in Sections 5–7. The total stress σ_1^{total} resulting from the superposition of these terms is discussed in Section 8.

2.3. Thermal history of PFCs

When the armour tiles of PFMs are attached to an actively cooled heat sink unit, steady state of heat flow and a corresponding stationary temperature profile will be established after a sufficient time period. This situation will occur during the operation of future fusion devices with long pulse discharges. A schematic of the temperature development of a PFC under typical fusion operation condition is shown in Fig. 2 [5].

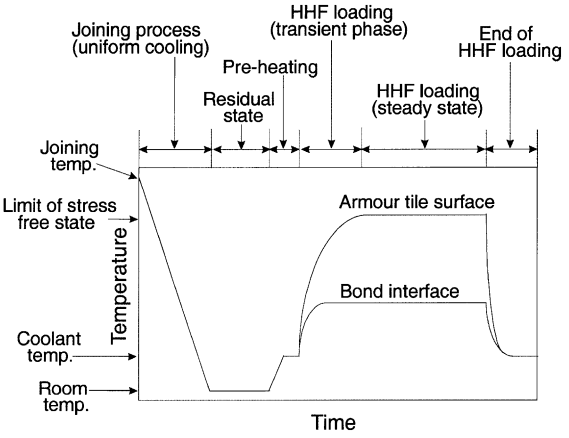

Fig. 2. Schematic of the temperature development in a PFC under typical fusion operation condition. (Two temperature curves are plotted each for the heating surface of armour tile and for bond interface, respectively.)

3. Materials

As a whole, five materials are used, that is, fine grain graphite (FU4206) and CFC (Sepcarb N112) for PFMs (i.e. armour tiles) whereas martensitic steel (9Cr1Mo), vanadium alloy (V4Cr4Ti) and copper alloy (CuCrZr) for the heat sink substrate. Hence, six material combinations consisting of two PFMs and three substrate materials are examined. This materials set is shown in Table 1.

The selected material properties are listed in Tables 2 and 3. In Table 3, the martensitic steel 9Cr1Mo steel has comparable thermal and mechanical properties to the low activation steels being currently under development. The reference load parameters used are given in Table 4.

The geometry of the joint model for the present analysis is shown in Fig. 3. In order to take the coolant

Table 1
Materials for the PFC joints considered for this analysis

Plasma facing armour tile	Graphite, CFC
Heat sink substrate	Copper alloy, martensitic steel, vanadium alloy

Table 2
Selected properties of the plasma facing materials at 300 °C [8–10]

	Graphite[a]	CFC[b]
Thermal conductivity (W/m K)	90	140
Thermal diffusivity (mm^2/s)	35.9	52
Thermal expansion coefficient (K^{-1})	5.2×10^{-6}	1.5×10^{-6}
Young's modulus (GPa)	10	28
Poisson's ratio	0.18	0.11
Nominal compressive strength (MPa)	90	160

[a] Quasi-isotropic.
[b] In-plane direction.

channel into account, the moment of inertia has to be calculated with which the corresponding effective thickness of the substrate can be determined.

4. Stress induced by temperature profile under full constraint

4.1. Thermal stress solution

Once the temperature profile has been obtained from a foregoing thermal analysis, the thermal stress of the armour tile for the boundary condition shown in Fig. 1(b) is determined applying the strain suppression method where full constraint by the heat sink is assumed [6]. This leads to

$$\sigma_1^{\mathrm{HHF}}(z) = \sigma_{1,x}(z) = -\frac{E_1\alpha_1[T(z) - T_0]}{1 - \nu_1}, \tag{2}$$

where E indicates the elastic modulus, ν is Poisson's ratio, and α is the coefficient of thermal expansion. The subscript 1 means material for the armour tile.

The stress solution given above is valid only for the bulk region distant from the lateral free surface due to Saint Venant's principle. This stress component is uniform in the in-plane direction.

To compute a precise temperature profile $T(z)$ including the transient phase, a numerical method considering realistic boundary conditions and temperature dependent material properties has to be applied. In this study, we use an analytical temperature solution so that we obtain a closed-form thermal stress solution. This closed-form solution will yield the first approximation but still maintaining the essential features of stress development.

To this end, we use a simplified thermal boundary condition. A model for thermal analysis of the armour tile is shown in Fig. 4. The top surface is heated by a prescribed constant, uniform heat flux Q_0 whereas the bottom plane is kept at a constant temperature of T_0 given a priori. This condition suggests that active cooling of the PFM tile takes place via the bond interface into the heat sink body. The heat flow will be nearly one-dimensional regardless of the detailed configuration of

Table 3
Selected properties of the substrate materials[a] [10,11]

	Martensitic steel	Vanadium alloy	Copper alloy
Coefficient of thermal expansion	11.5×10^{-6}	10×10^{-6}	17.6×10^{-6}
Young's modulus (GPa)	188	130	115
Poisson's ratio	0.3	0.36	0.33
Yield stress (MPa)	400 (500 °C)	262	245

[a] Listed data are for temperature of 300 °C.

Table 4
Loading parameters used for this analysis

Boundary conditions	Without bending, active cooling
Heat flux (Q_0)	5 MW/m^2
Heat load duration (t)	10 s
Interface temperature (T_0)	320 °C
Thickness of the armour tile	10 mm
Thickness of the substrate[a]	10 000 mm

[a] The thickness of heat sink substrate is chosen somewhat arbitrarily. With this thickness ratio, it is assumed that the metallic substrate possesses a sufficiently large moment of inertia so that thermally induced bending of the joint structure is suppressed.

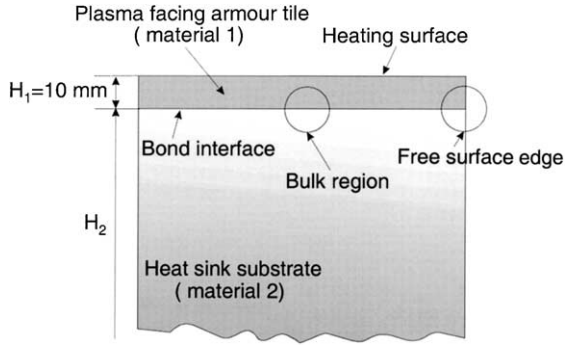

Fig. 3. Geometry of the joint model used for the present analysis.

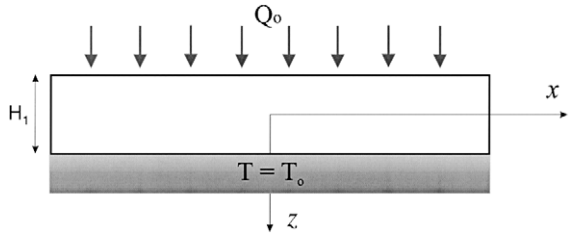

Fig. 4. Geometry and boundary condition for thermal analysis.

the heat sink system. Thus, the temperature profile and the resulting thermal stress will be a function only of the vertical position. In this work, 300 °C is assumed for T_0. In real situations, the contact interface will experience varying temperature during transient phase and attains a stationary value, which will be determined by the heat removal rate via coolant.

The pertinent analytical solution for the present problem is [12]

$$T = \frac{2Q_0\sqrt{\kappa t}}{K} \times \sum_{n=0}^{\infty}(-1)^n \left[\operatorname{ierfc}\frac{(2n+1)H_1 - (H_1/2 - z)}{2\sqrt{\kappa t}} - \operatorname{ierfc}\frac{(2n+1)H_1 + (H_1/2 - z)}{2\sqrt{\kappa t}}\right] + T_0 \tag{3a}$$

$$= \frac{Q_0(H_1/2 - z)}{K} - \frac{8Q_0H_1}{K\pi^2}\sum_{n=0}^{\infty}\frac{(-1)^n}{(2n+1)^2} \times \mathrm{e}^{-\kappa(2n+1)^2\pi^2 t/4H_1^2}\sin\frac{(2n+1)\pi(H_1/2 - z)}{2H_1} + T_0, \tag{3b}$$

for which the heat flux is Q_0 at $z = -H_1/2$ and $T = T_0$ at $z = H_1/2$ being kept constant for $t > 0$. This solution is exactly valid only for thermal properties being independent of temperature.

Substituting the temperature solution (3a), (3b) into the stress solution (2) yields

$$\sigma_1^{\text{gradient}}(z) = -\frac{E_1\alpha_1}{1-\nu_1}\left[\frac{Q_0(H_1/2 - z)}{K} - \frac{8Q_0H_1}{K\pi^2} \times \sum_{n=0}^{\infty}\frac{(-1)^n}{(2n+1)^2}\mathrm{e}^{-\kappa(2n+1)^2\pi^2 t/4H_1^2} \sin\frac{(2n+1)\pi(H_1/2 - z)}{2H_1}\right] \tag{4}$$

In Eq. (4), the constant interface temperature T_0 is not included anymore. Hence, in order to utilise the analytical stress solution for σ_1^{HHF}, one does not need to know the interface temperature a priori.

Table 5
Maximum thermal stress values of armour tiles for several PFMs induced by temperature profile in them

Armour tile materials	Stress by temperature profile in armour tile, σ_1^{HHF} (MPa)	Surface temperature (°C)
Graphite	0[a]	856
	−35[b]	
CFC	0[a]	657
	−16[b]	

Active cooling, heat flux: 5 $\mathrm{MW/m^2}$, HHF load duration: 10 s, thickness: 10 mm.
[a] Stress at the interface of the armour tile.
[b] Stress at the heated surface of the armour tile.

4.2. Results for several PFMs

Results for the stress σ_1^{HHF} are listed in Table 5. The stress portion σ_1^{HHF} of the graphite tile is much smaller than CFC due to its low elastic modulus despite the much higher peak temperature. Since the applied constraint is the suppression of a thermal expansion, the stresses are compressive. The stress distributions reflect the temperature profiles proportionally.

5. Stress by mismatch of thermal strain – elastic case

Since the duplex joint structure consisting of different materials has been one of the most preferred design concepts for PFCs, thermal stress arising from the misfit of differential thermal expansion of member materials is of fundamental importance. Actually, this stress contribution can be still more significant than that of the temperature gradient. In addition, the residual stress is also to be considered which stems from the joining process of the component. Since the residual stress is generated by cooling from the processing temperature, the subsequent heating can result in stress reduction depending on the stress free temperature. The high strain energy coupled with instantaneous residual stress often leads to cracking of the bond interface. Hence, the precise prediction of the residual stress state of the interface is important for the assessment of component integrity.

In this section, this mismatch stress is discussed considering both the PFMs and the substrate as linear-elastic, subject to the premise that bonding is conducted at a certain elevated temperature. A theoretical tool is introduced with which the actual stress is obtained for a given temperature difference between the stress free state and the instantaneous state (e.g. room temperature or operational temperature of the interface). The thickness of the armour tile is assumed to be 10 mm and that of substrate, 10 000 mm.

5.1. Mismatch thermal stress in armour tile

The simple analytical solution given by Hsueh and Evans [7], which is based on the method of Timoshenko [2], describes the thermal stress distribution along the thickness of joint materials. This solution is valid only for the bulk region distant from the free surface edge of the bond interface, since the assumption of the Bernoulli beam theory was applied to this solution [2].

In the schematic representation of joint model given in Fig. 3, the bulk – and the free surface edge region are denoted, respectively.

The mismatch thermal stress in the armour tile can be described by

$$\sigma_{1,\mathrm{el}}^{\mathrm{mismatch}}(\tilde{z}) = E_1^*\left[\varepsilon_0^{\mathrm{el}} + (\alpha_2-\alpha_1)\Delta T\right] + E_1^*\left(\tilde{z} - t_n^{\mathrm{el}}\right)/\rho^{\mathrm{el}}, \tag{5}$$

in which the vertical co-ordinate $\tilde{z}$ has the value, $\tilde{z}=0$ at the interface and $\tilde{z}=H_1$ at the heating surface. The individual parameters are given by

$$\varepsilon_0^{\mathrm{el}} = \frac{E_1^*(\alpha_1-\alpha_2)\Delta T H_1}{2(E_1^*H_1+E_2^*H_2)}, \tag{6}$$

$$t_n^{\mathrm{el}} = \frac{E_1^*H_1^2 - E_2^*H_2^2}{2(E_1^*H_1+E_2^*H_2)}, \tag{7}$$

$$\rho^{\mathrm{el}} = \frac{E_1^{*2}H_1^4 + E_2^{*2}H_2^4 + 2E_1^*E_2^*H_1H_2\left(2H_1^2+2H_2^2+3H_1H_2\right)}{6E_1^*E_2^*H_1H_2(H_1+H_2)(\alpha_1-\alpha_2)\Delta T}, \tag{8}$$

where the subscripts 1 and 2 denote the PFM and the substrate, H_i the thickness of each material, ΔT the instantaneous temperature difference from the stress free state, ε_0 a characteristic constant, t_n the position of the neutral axis and ρ is the radius of curvature of the joint, respectively. The effective moduli E_i^* take either E_i for plane stress condition or $E_i/(1-\nu_i)$ for plane strain condition.

The maximum stress of PFM is located at the material interface and is found to be

$$\sigma_{\max}^{\mathrm{mismatch}} = \frac{1}{\rho}\left[\frac{2\left(E_1^*I_1+E_2^*I_2\right)}{H_1(H_1+H_2)} + \frac{1}{2}E_1^*H_1\right], \tag{9}$$

where the moment of inertia I_i of the individual layers is given by $I_i = H_i^3/12$.

The bulk interfacial stress is directly proportional to the misfit of the CTEs and ΔT . It depends weakly on the mismatch of the elastic modulus.

The resultant mismatch stress will be dependent on the stress free temperature. If the temperature of the stress free state lies below the instantaneous temperature of the interface, then the sign of the stress will change. The interface stress as well as the surface stress depends only on the thickness ratio of the layers. As a natural consequence, if the thickness ratio is fixed, the thickness itself does not affect the absolute stress level but just the gradient of it.

The classical solution for the mismatch stress fields will break down in the vicinity of the traction free surface. There often occurs, but not necessarily, singular stress concentration near the free surface edge of the interface. This multi-axial singular stress fields which are bounded normally in a small region are often the cause of material failure. In a global scale, the in-plane thermal stress component at the free surface distant from the interface should vanish (normal stress component must be null at the traction free surface). Thus, the mismatch thermal stress occurring in the neighbourhood of the free surface but distant from the singular stress fields must be weaker than that of the bulk region.

6. Stress by mismatch of thermal strain – plastic case

In case of a ductile heat sink substrate, plastic flow can take place during the joining process or subsequent heat loading. The plastic flow initiates at the bond interface of the substrate. The concomitant stress redistribution caused by the plastic relaxation can be estimated through incremental stress updating. Once the metallic part begins to yield, the mismatch stress of PFMs in the armour tile cannot increase in proportion. As a result, the stress evolution of PFMs will be alleviated in comparison to the elastic case.

In this section, a plastic stress solution for a bond joint is introduced which was developed by Hsueh and Evans [7]. As in the previous sections, the mismatch stress only of the armour tile is treated. It is usual that the plastic deformation is localised in the neighbourhood of the interface. Such a partial-plastic condition requires the determination of the yielding front.

In principle, the plastic yielding can occur either during the cooling process following bonding or during subsequent thermal loading, depending on the temperature difference during the thermal sequence. In this work, we assume that the yielding occurs only during the cooling process and that the metallic substrate remains in the elastic range during the following thermal loading. This premise may reasonably represent the actual thermo-mechanical history experienced by a PFC, since the temperature at the joint interface during HHF loading is much lower than the stress free temperature. In addition, the existence of the residual stress field suppresses the yield significantly during subsequent thermal loading.

To compute the resultant mismatch stress, we apply the superposition method again. The resultant mismatch stress of the armour at any instant of HHF loading can be obtained by adding the residual stress after cooling and the secondary stress upon re-heating as follows:

$$\sigma_{1,\mathrm{pl}}^{\mathrm{mismatch}} = \sigma_{1,\mathrm{pl}}^{\mathrm{residual}} + \sigma_{1,\mathrm{el}}^{\mathrm{reheating}}. \tag{10}$$

6.1. Residual mismatch thermal stress in an armour tile with substrate yielding

In case of partial-plastic yielding of the substrate, the residual mismatch thermal stress in the armour tile can be described by

$$\sigma_{1,\mathrm{pl}}^{\mathrm{residual}}(\tilde{z}) = E_1^*\left[\varepsilon_0^{\mathrm{pl}} + (\alpha_2-\alpha_1)\Delta T_{\mathrm{c}}\right] + E_1^*\left(\tilde{z} - t_n^{\mathrm{pl}}\right)/\rho^{\mathrm{pl}}, \tag{11}$$

in which the vertical co-ordinate $\tilde{z}$ has the same convention as in Section 5 and ΔT_{c} is the temperature change on cooling.

For large work hardening rate ($H_p \to \infty$), the individual parameters are given by

$$\varepsilon_0^{\mathrm{pl}} = \frac{1}{2\rho^{\mathrm{pl}}}\frac{E_1^*H_1\left(H_1+2h_y\right) - E_2^*H_2\left(H_2-2h_y\right)}{E_1^*H_1 + E_2^*H_2} + \frac{\sigma_y}{E_2^*}, \tag{12}$$

$$t_n^{\mathrm{pl}} = \frac{E_1^*H_1^2 - E_2^*H_2^2}{2\left(E_1^*H_1 + E_2^*H_2\right)}, \tag{13}$$

$$\rho^{\mathrm{pl}} = \frac{E_1^{*2}H_1^4 + E_2^{*2}H_2^4 + 2E_1^*E_2^*H_1H_2\left(2H_1^2+2H_2^2+3H_1H_2\right)}{6E_1^*E_2^*H_1H_2(H_1+H_2)(\alpha_1-\alpha_2)\Delta T_{\mathrm{c}}}, \tag{14}$$

$$h_y = \left\{\left[E_1^{*2}H_1^4 + E_2^{*2}H_2^4 + 2E_1^*E_2^*H_1H_2\left(2H_1^2+2H_2^2+3H_1H_2\right)\right]\sigma_y + E_1^*E_2^*\left[E_1^*H_1^4 + E_2^*H_2^2H_1(3H_1+4H_2)\right]\times(\alpha_2-\alpha_1)\Delta T_{\mathrm{c}}\right\}\Big/6E_1^{*2}E_2^*H_1H_2(H_1+H_2)(\alpha_2-\alpha_1)\Delta T_{\mathrm{c}}, \tag{15}$$

where h_y is the position of the yield front, i.e., the elastic/plastic boundary, and for perfect plasticity ($H_p \to 0$),

$$\varepsilon_0^{\mathrm{pl}} = \frac{1}{2\rho^{\mathrm{pl}}}\frac{E_1^*H_1\left(H_1+2h_y\right) - E_2^*\left(H_2-h_y\right)^2}{E_1^*H_1 + E_2^*\left(H_2-h_y\right)}, \tag{16}$$

$$t_n^{\mathrm{pl}} = \frac{1}{2}\frac{E_1^*H_1^2 - E_2^*\left(H_2^2-h_y^2\right)}{E_1^*H_1 + E_2^*\left(H_2-h_y\right)}, \tag{17}$$

$$\rho^{\mathrm{pl}} = \frac{1}{2}\frac{E_2^{*2}\left(H_2-h_y\right)^2 - E_1^*E_2^*H_1\left(H_1+2h_y\right)}{\left(E_1^*H_1+E_2^*H_2\right)\sigma_y + E_1^*E_2^*H_1(\alpha_2-\alpha_1)\Delta T_{\mathrm{c}}}, \tag{18}$$

$$\begin{aligned}&\left[E_1^{*2}H_1^4 + E_2^{*2}H_2^4 + 2E_1^*E_2^*H_1H_2\left(2H_1^2+2H_2^2+3H_1H_2\right)\right]\sigma_y \\ &+ \left[2h_y\left(E_1^*H_1+E_2^*H_2\right) - 3\left(E_2^*H_2^2 - E_1^*H_1^2\right)\right]E_2^*h_y^2\sigma_y \\ &= E_1^*E_2^*(\alpha_2-\alpha_1)\Delta T_{\mathrm{c}}\left[-H_1\left(E_1^*H_1^3 + 3E_2^*H_2^2H_1 + 4E_2^*H_2^3\right)\right. \\ &\left. + 6E_2^*H_1H_2h_y(H_1+H_2) - E_2^*H_1h_y^2\left(2h_y+3H_1\right)\right].\end{aligned} \tag{19}$$

In Eq. (19), the yield front h_y in a perfect-plastic substrate is determined by solving this polynomial equation.

6.2. Secondary mismatch thermal stress in armour tiles upon re-heating with HHF load

Having assumed that plastic yielding is suppressed during re-heating, the secondary mismatch thermal stress in the armour tile that develop during re-heating can be computed using the elastic solution, Eqs. (5)–(8) replacing ΔT with ΔT_{h}, where ΔT_{h} is the temperature change at the bond interface on re-heating having a positive value

$$\sigma_{1,\mathrm{el}}^{\mathrm{reheating}}\left(\tilde{z}\right) = E_1^*\left[\varepsilon_0^{\mathrm{el}} + (\alpha_2-\alpha_1)\Delta T_{\mathrm{h}}\right] + E_1^*\left(\tilde{z} - t_n^{\mathrm{el}}\right)/\rho^{\mathrm{el}}. \tag{20}$$

7. Results of mismatch stress of armour tiles

A series of calculations is presented in this section, for a specific temperature history in order to make a comparison between the elastic and elasto-plastic model. For all calculations, it is assumed that the joint components are cooled from an arbitrary stress free temperature of 620 °C to a reference temperature (room temperature). Subsequently, they are subjected to further HHF load (this subsequent HHF loading is termed as re-heating in the following) with increasing interface temperature up to the steady-state value of 320 °C. The assumed temperature values both for the stress free state and the steady state are taken from the data for a typical brazed plasma facing component under normal operation [13].

In the elastic analysis, the determining quantity is the temperature difference ΔT between the stress free state and the steady state, which is 300 °C in the present case. For elasto-plastic analysis, the temperature decrease on cooling (ΔT_{c}) and the increase on re-heating (ΔT_{h}) are −600 and 300 °C, respectively. The yield stresses of the substrate materials are taken from Table 3.

The results for plane strain condition are summarised in Table 6. The mismatch stress values are given both for the heating surface of the armour tile and for the interface on the armour side. In this table, three stress states are presented, that is, residual stress $\sigma_{1,\mathrm{el}}^{\mathrm{residual}}$ from the elastic calculation, residual stress $\sigma_{1,\mathrm{pl}}^{\mathrm{residual}}$ from the elasto-plastic estimation and the subsequent mismatch stress $\sigma_{1,\mathrm{pl}}^{\mathrm{mismatch}}$ in steady state on re-heating, which was obtained using $\sigma_{1,\mathrm{pl}}^{\mathrm{residual}}$.

The results show that the graphite tile experiences a considerably smaller mismatch stress than the CFC tile. This is mainly due to the low stiffness and small CTE misfit of graphite for metallic heat sinks. Nevertheless, the strength margin for graphite tile seems to be not

Table 6
Mismatch thermal stresses of the armour tiles bonded to various heat sink substrate materials

Joints		Residual stress (elastic)	Residual stress (elasto-plastic)	Mismatch HHF stress (elasto-plastic)
Heat sink	Armour tile			
Copper alloy	Graphite	−90[a]	−90[a]	−45[a]
		−90[b]	−90[b]	−45[b]
	CFC	−304[a]	−304[a]	−152[a]
		−304[b]	−304[b]	−152[b]
Martensitic steel	Graphite	−46[a]	−46[a]	23[a]
		−46[b]	−46[b]	−23[b]
	CFC	−188[a]	−188[a]	−94[a]
		−188[b]	−188[b]	−94[b]s
Vanadium alloy	Graphite	−35[a]	−35[a]	−18[a]
		−35[b]	−35[b]	−18[b]
	CFC	−160[a]	−160[a]	−80[a]
		−160[b]	−160[b]	−80[b]

Both the residual stresses at room temperature and thermal stress in the steady state during the subsequent HHF re-heating are listed. Interface temperature on re-heating: 320 °C, temperature change on cooling: −600 °C.
[a] Stress at the interface of the armour tile.
[b] Stress at the heated surface of the armour tile.

sufficient. The stress for the graphite–copper joint already reached the mean compressive strength of graphite (90 MPa). For the graphite tiles of other joints, which show lower residual stresses than 90 MPa, statistical failure prediction is necessary using the Weibull parameter.

The CFC-copper joint experiences a more significant residual stress than any other joints. Residual stresses of the CFC tiles for all joints exceeded the mean compressive strength of Sepcarb N112 (160 MPa).

On the other hand, the compressive residual stress states have a beneficial aspect, since spontaneous dynamic fracture is suppressed. Instead, brittle damage will be accumulated under repeated compression.

Another important feature is that no plastic relaxation is predicted for all joints. The mismatch stress occurring in the metallic substrate is much lower than that in the armour tile, since the substrate was assumed to have a much larger dimension than the armour tile. Hence, the stresses do not exceed the elastic limit. Remarkable plastic stress relaxation will occur, if the substrate thickness is reduced. Then, the substrate stress can be high enough to exceed the yield stress. Such a case can probably occur in the practice of manufacturing, since the substrate thickness of a component module for bonding process will be normally much smaller than that of in-vessel PFC structures. An essential limitation of the present procedure to compute the plastic relaxation on cooling is that the temperature dependence of the yield strength cannot be taken into account. To solve this restriction, an incremental algorithm may be applied.

The mismatch stresses are uniform in the whole tile thickness which indicates that the bending is completely suppressed. The change of mismatch stress in the armour tiles during the re-heating stage can be determined from the difference between $\sigma_{1,\mathrm{pl}}^{\mathrm{residual}}$ and $\sigma_{1,\mathrm{pl}}^{\mathrm{mismatch}}$. A common feature is that the relaxation of the mismatch stress is proportional to temperature increase, as can be readily expected.

8. Total thermal stress during plasma operation

For the assessment of the failure mechanism, the total resultant stress has to be estimated by superposition of all stress contributions. The final results of the resultant total thermal stress of the armour tiles are summarised in Table 7. The values are obtained by summation of the results in Table 5 with those in Table 6.

During HHF loading the heated surface undergoes higher compression stress than interface region. In most cases, the stresses in the whole tile domain are relieved on HHF loading. However, in the armour tiles of the graphite–steel and the graphite–vanadium joints, stresses at the heated surface increase during HHF loading. Interface stresses decrease during HHF loading in all joints. Hence, interfacial failure will occur during the cooling phase. Surface damage can be relieved or enhanced on re-heating depending on the material combinations. In all joints, the armour tile experiences a cyclic thermal stress variation during a HHF loading cycle. Therefore, repeated re-heating can lead to a fatigue failure of the tile even for the case of low peak stress. Stress gradient in the armour tiles of all joints originates solely from σ_1^{HHF}, since no actual bending is generated by mismatch stress. It has to be noted that all

Table 7
Resultant total thermal stresses at the heated surface and at the interface of the armour tile in steady state of the HHF re-heating

Joints		Residual stress (elasto-plastic)	Total HHF stress (elasto-plastic)
Heat sink	Armour tile		
Copper alloy	Graphite	−90[a]	−45[a]
		−90[b]	−80[b]
	CFC	−304[a]	−152[b]
		−304[b]	−168[b]
Martensitic steel	Graphite	− 46[a]	−23[a]
		−46[b]	−58[b]
	CFC	−188[a]	−94[a]
		−188[b]	−110[b]
Vanadium alloy	Graphite	−35[a]	−18[a]
		−35[b]	−53[b]
	CFC	−160[a]	−80[b]
		−160[b]	−96[b]

For comparison, the residual stresses are also given. Effective temperature change on cooling: −600 °C, interface temperature on re-heasting: 320 °C, HHF load: 5 MW/m^2.
[a] Stress at the interface of the armour tile.
[b] Stress at the heated surface of the armour tile.

results presented here are based on the specific thermal history which was employed as an example.

9. Concluding remarks

In this article, a comprehensive analytical model was presented for the assessment of thermal stress of armour tiles of plasma facing components under HHF load. It was assumed that a 10 mm thick plasma facing armour tile is bonded to a thick heat sink substrate at a certain process temperature (620 °C). It was further assumed that this joint is cooled to room temperature and subsequently subjected to a high heat flux load (5 MW/m^2) imposed onto the armour tile surface. Active cooling is considered. These premises approximate the real loading scenario experienced by a plasma facing component under fusion operation.

The resultant thermal stresses were formulated in a closed-form solution. To achieve it, it was supposed that the resultant thermal stress consists of three constituting stress contributions each having different origins. These three stress terms are: residual mismatch stress from bonding process, mismatch stress by re-heating upon high heat flux loading and thermal stress by the temperature profile in the tile during HHF loading, respectively. The method of stress superposition was applied to obtain the total resultant thermal stress from these individual stress portions. Emphasis is put on the modelling capability of the plastic relaxation of metallic substrate. It was supposed that plastic yielding can occur only during the cooling process.

Stress analysis was performed for joints with six different material combinations which are of technical importance in fusion engineering. The predicted stress response of the armour tiles showed a trend which was consistent with physical interpretation. It was shown that no plastic deformation occurs during the cooling process, if the thickness of the heat sink structure is much larger than that of the tiles. However, plastic relaxation may be important when the substrate of the component module for the bonding process has a much smaller thickness than the actual in-vessel built-in substrate.

The results of this comparative study can provide us with a criterion on materials screening and an understanding of the stress generation and failure mechanism. The present analytical procedure enables us to perform a simple estimation of thermal stress for plasma facing components without employing any sophisticated numerical tool.

Acknowledgements

We are grateful to Dr Hsueh and Mr Krempaszky for the helpful discussion.

Appendix A.

Sometimes it may be interesting to separate the thermal stress σ_1^{HHF} in components again. For this, it is worthwhile to scrutinise the imaginary boundary condition of Fig. 1(b) in detail. The stress σ_1^{HHF} for this boundary condition can be divided into two contributions considering the following additive superposition:

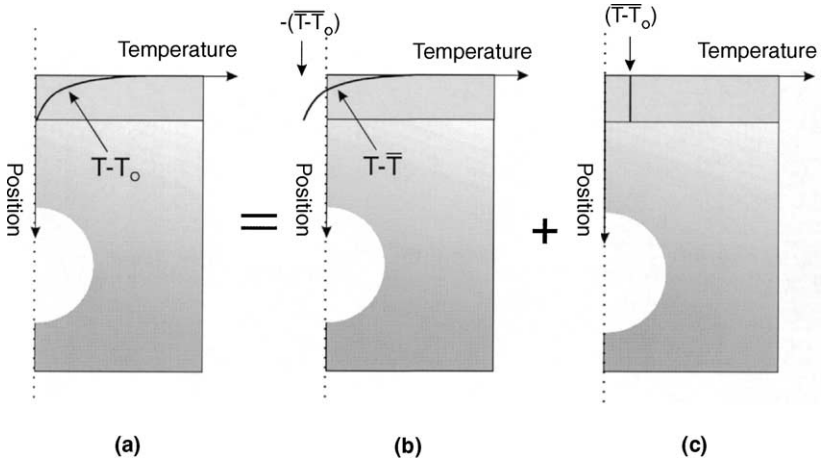

Fig. 5. Schematic of two virtual boundary conditions for constituent stress portions which are superposed to produce thermal stress due to temperature profile in armour tiles under full strain suppression.

$$\sigma_1^{\mathrm{HHF}} = \sigma_1^{\mathrm{gradient}} + \sigma_1^{(\overline{T-T_0})}. \tag{A.1}$$

The second term $\sigma_1^{\mathrm{gradient}}$ indicates the stress induced purely by the relative temperature gradient in the armour tile whereas the third term $\sigma_1^{(\overline{T-T_0})}$ is the stress due to the bonding constraint against in-plane expansion of the tile which is caused by the average temperature difference between the armour tile ($\overline{T}$) and the heat sink (T_0).

This relation is illustrated in Fig. 5. The boundary condition (b) corresponds to the stress portion $\sigma_1^{\mathrm{gradient}}$ whereas that of (c) stands for the stress portion $\sigma_1^{(\overline{T-T_0})}$, respectively. In Fig. 5(b), the whole temperature profile $T - T_0$ is subtracted by its average value, $\overline{T - T_0}$, so that the mean temperature of this new profile is equal to null (i.e. the first statistical moment vanishes). In this case, there will be no net in-plane thermal expansion. Now, one obtains thermal stress only due to the temperature inhomogeneity in the tile under bending constraint by the substrate. In Fig. 5(c), the relative in-plane thermal expansion of the armour tile is characterised by the average temperature difference $\overline{T - T_0}$ (or $\bar{T} - T_0$). Since the stress term $\sigma_1^{(\overline{T-T_0})}$ is produced actually by bonding constraint, it can be estimated in an analogous manner as the mismatch thermal stress.

The thermal stress for the boundary condition of Fig. 5(b) is calculated by [6]

$$\begin{aligned}\sigma_1^{\mathrm{gradient}}(z) &= \sigma_{1,x}(z) \\ &= -\frac{E_1\alpha_1\left[T(z) - T_0 - \left(\overline{T}(z) - T_0\right)\right]}{1 - \nu_1} \\ &= -\frac{E_1\alpha_1\left[T(z) - \overline{T}(z)\right]}{1 - \nu_1},\end{aligned} \tag{A.2}$$

$$\overline{T}(z) = \frac{1}{H_1}\int_{-H_1/2}^{H_1/2} T(z)\,\mathrm{d}z, \tag{A.3}$$

where the relation $T(z) - T_0(z) - [\overline{T}(z) - T_0(z)] = T(z) - \overline{T}(z)$ is used and no bending of the armour tile is assumed.

The stress solution Eq. (A.2) can be appreciated from a different angle by considering an alternative boundary condition which is mechanically equivalent to Fig. 5(b). This situation is illustrated in Fig. 6. After substituting Eq. (A.3) into Eq. (A.2) and re-arranging, we obtain

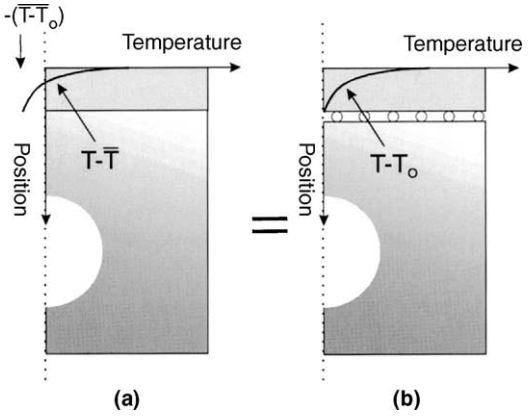

Fig. 6. Schematic of two boundary conditions for thermal stress generated purely by temperature gradient which are mechanically equivalent. The thermal stresses occurring in these armour tiles are identical. (Only the symmetric half of a component cross-section is shown.)

$$\sigma_1^{\text{gradient}}(z) = \sigma_{1,x}(z) = -\frac{E\alpha T(z)}{1-\nu} + \frac{1}{H_1(1-\nu)} \times \int_{-H_1/2}^{H_1/2} E\alpha T(z)\,\mathrm{d}z. \quad (A.4)$$

This equation corresponds to the stress solution for the boundary condition of Fig. 6(b), in which the form of the temperature profile is identical to that of (a) differing only by the constant average temperature $\overline{T}$ and the mechanical constraint is imposed only against bending still allowing free expansion. The last term of the solution can be interpreted as the mean value of the original stress in Eq. (2) with the opposite sign. With this additional stress term, any in-plane external force (surface traction) is removed.

This demonstrates the mechanical equivalence of the two boundary conditions (a) and (b) in Fig. 6. Now, it is clear that the stress solution, Eq. (A.2), for $\sigma_1^{\text{gradient}}$ actually stands for the stress portion purely by the relative temperature gradient without constraint against in-plane thermal expansion.

The stress $\sigma_1^{\overline{(T-T_0)}}$ for the boundary condition of Fig. 5(c) is obtained by

$$\sigma_1^{\overline{(T-T_0)}} = -\overline{(T-T_0)}E_1\alpha_1/(1-\nu_1). \quad (A.5)$$

Substituting Eqs. (A.2), (A.5) and (2) into (A.1) verifies that the superposition relation is satisfied.

References

[1] K. Ioki, T. Garching, J. Nucl. Mater. 258–263 (1998) 74.
[2] S. Timoshenko, J. Opt. Soc. Am. 11 (1925) 233.
[3] J.H. You, J. Mater. Eng. Perform. 7 (1998) 114.
[4] J.H. You, G. Breitbach, Fus. Eng. Des. 38 (1998) 307.
[5] J.H. You, H. Bolt, R. Duwe, J. Linke, H. Nickel, J. Nucl. Mater. 250 (1997) 184.
[6] S. Timoshenko, J.N. Goodier, Theory of Elasticity, 3rd Ed., McGraw-Hill, New York, 1970.
[7] C.H. Hsueh, A.G. Evans, J. Am. Ceram. Soc. 68 (1985) 241.
[8] W. Delle, J. Linke, H. Nickel, E. Wallura, Spezielle Berichte der KFA Jülich, Jül-Spez-401, 1987.
[9] I. Smid, M. Akiba, M. Araki, S. Suzuki, K. Satoh, JAERI Report, Japan Atomic Energy Research Institute, JAERI-M 93-149, 1993.
[10] ITER Material Properties Handbook, ITER Document No. S74RE1.
[11] A.F. Tavassoli, J. Nucl. Mater. 258–263 (1998) 85.
[12] H.S. Carslaw, J.C. Jaeger, Conduction of Heat in Solids, 2nd Ed., Oxford University, Oxford, 1959.
[13] R. Matera, G. Federici, ITER JCT, J. Nucl. Mater. 233–237 (1996) 17.